Electronic Supplementary Material (ESI) for Catalysis Science & Technology.

Supplementary Information

Altering the influence of ceria oxygen vacancies in $Ni/Ce_xSi_yO_2$ for photothermal CO_2 methanation

Salina Jantarang, Emma C. Lovell*, Tze Hao Tan, Bingqiao Xie, Jason Scott*, Rose Amal

Particles and Catalysis Research Group, School of Chemical Engineering, The University of New South Wales, Sydney, NSW 2052, Australia
* Corresponding authors: e.lovell@unsw.edu.au, jason.scott@unsw.edu.au

List of Figures and Tables

Catalyst Properties

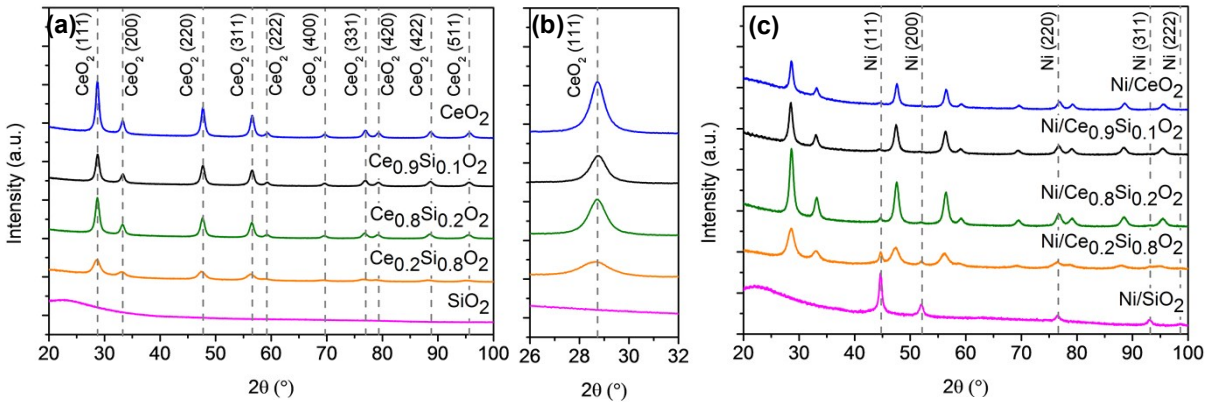

Figure S1 *XRD patterns of $Ce_xSi_yO_2$ from (a) 20 ° - 100 ° and (b) magnified spectra between 26 ° - 32 °. The Miller indices of CeO_2 were referenced to JCPDS: 01-083-9465. The XRD patterns of (c) reduced and passivated Ni/$Ce_xSi_yO_2$ were recorded from 20 ° - 100 °; JCPDS: 04-016-4592 (Ni).*

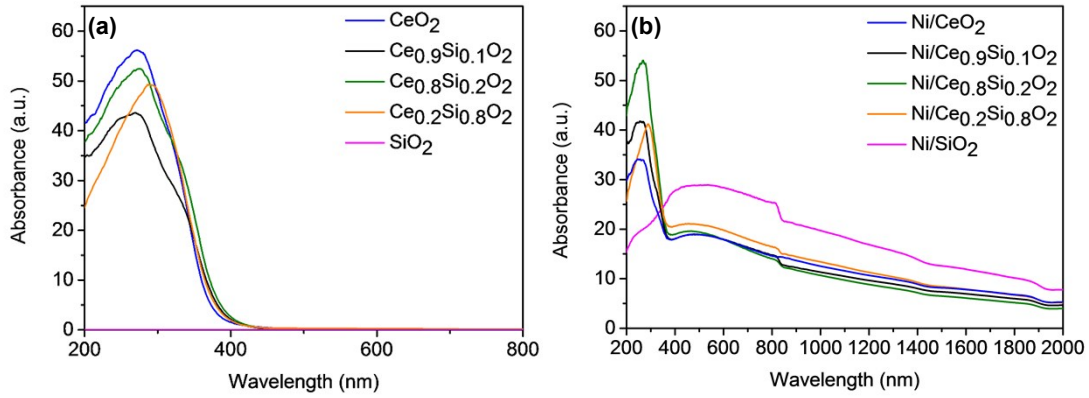

Figure S2 *(a) UV-vis absorbance of $Ce_xSi_yO_2$ from 200 – 800 nm. (b) UV-vis-NIR absorbance of reduced and passivated Ni/$Ce_xSi_yO_2$ from 200 – 2000 nm. The absorption peak at 830 nm is due to the instrument.*

Table S1 *Actual Ni loading as determined from ICP-OES of as-prepared Ni/$Ce_xSi_yO_2$. The Ni catalysts have a nominal loading of 10 wt.%.*

Catalyst	Actual Ni loading (wt.%)
Ni/CeO_2	8.7
$Ni/Ce_{0.9}Si_{0.1}O_2$	9.7
$Ni/Ce_{0.8}Si_{0.2}O_2$	10.1
$Ni/Ce_{0.2}Si_{0.8}O_2$	9.4
Ni/SiO_2	9.1

Thermogravimetric analysis of SiO_2 was performed on a TGA Q5000 (TA instruments) under a flow of dry compressed air from 50 °C – 800 °C, ramped at 20 °C/min. The SiO_2 (~ 2 mg) was analysed using a platinum pan. SiO_2 was selected for TGA analysis as it had the highest specific surface area where any weight loss from residual carbon is most likely to be observed. The TGA shows ≈ 6% up to 500 °C (due to water and dehydroxylation) with negligible loss observed > 500 °C. The catalysts were all calcined at 400 °C and reduced at 500 °C. The weight loss difference between 400 °C – 500 °C is ≈ 0.5%. Hence, the catalyst preparation conditions reached temperatures beyond the point where any further mass loss occurred. However, the presence of carbon species on the catalyst surface due to adsorption upon exposure to the atmosphere is likely. XPS C 1s spectra show that carbon specie were present on the catalyst surface, which may originate from the atmospheric adsorption (**Figure S6**).

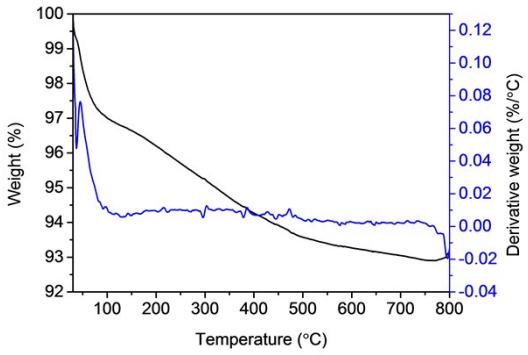

Figure S3 *Thermogravimetric analysis of SiO_2 showing weight loss over the range 50 °C – 800 °C*

Defects and oxygen vacancies were identified using electron paramagnetic resonance (EPR) on a Bruker EMX X-Band ESR Spectrometer operated at frequency of approximately 9.43 GHz. The samples (20 mg) were loaded into a 4 mm (internal diameter) quartz tube and characterised at -153 °C, with the system cooled by liquid nitrogen. Raman spectra were collected at 25 MW using a 514 nm laser on a Renishaw inVia Raman Microscope.

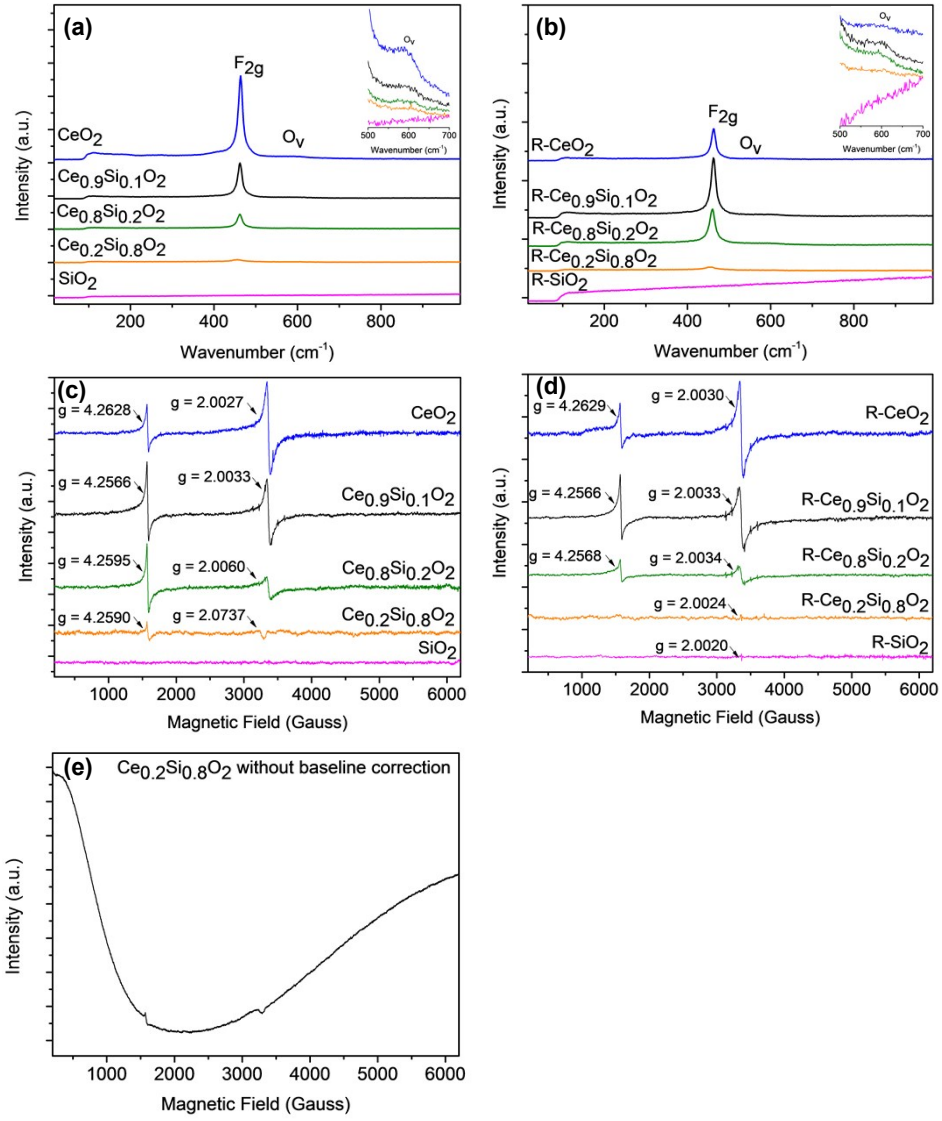

Figure S4 *Raman spectra of (a) as-prepared and (b) reduced $Ce_xSi_yO_2$. Inset shows magnified spectra over the range 500 – 700 cm^{-1}. Peak at approximately 464 cm^{-1} corresponds to the F_{2g} mode of CeO_2 (symmetrical stretching of Ce-O) while the broad peak between 500 cm^{-1} to 600 cm^{-1} confirms the presence of oxygen vacancies.[1–5] EPR spectra of (c) as-prepared $Ce_xSi_yO_2$, (d) reduced $Ce_xSi_yO_2$ and (e) $Ce_{0.2}Si_{0.8}O_2$ without baseline correction, only observed for as-prepared and reduced $Ce_{0.2}Si_{0.8}O_2$.*

Fourier-transform infrared (FTIR) spectra were collected using a Spotlight 400 FTIR (PerkinElmer) from 600 – 4000 cm^{-1} under ambient conditions with scan resolution of 4 cm^{-1} with 8 scans per spectrum.

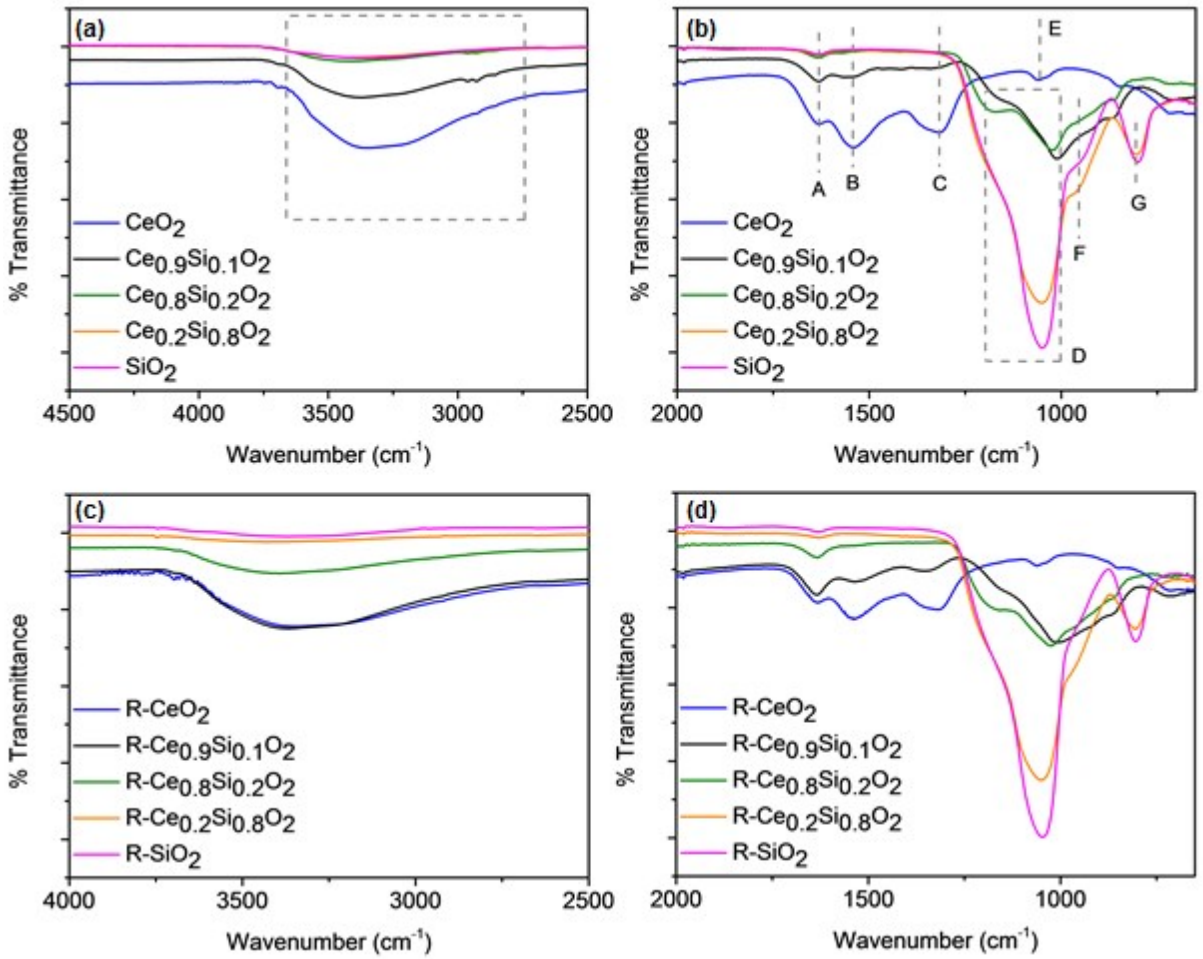

Figure S5 *FTIR spectra of as-prepared and reduced (R) $Ce_xSi_yO_2$ from (a,c) 4500 - 2500 cm^{-1} and (b,d) 2000 – 650 cm^{-1}, respectively. The broad peak region between 3750 cm^{-1} – 2750 cm^{-1} for both CeO_2 and SiO_2 indicate water adsorption.*[1,6,7] *In the CeO_2 spectrum, the peak at 1319 cm^{-1} (C) corresponds to stretching vibrational mode Ce-O-Ce* [8]*, the peak at 1628 cm^{-1} (A) is attributed to the O-H deformation vibration*[8]*. The SiO_2 sampled exhibited peaks at (D) 1049 cm^{-1}, asymmetric stretch (Si-O-Si), and (G) 801 cm^{-1}, symmetric stretch (Si-O-Si).*[7]

The oxidation states and shifts in binding energies of the elements present in the reduced and passivated Ni catalysts were studied via X-ray photoelectron spectroscopy (XPS) using an ESCALAB 250Xi (Thermo Scientific) with an Al Kα X-ray source. The binding energies of the spectra were referenced to carbon 1s at 284.8 eV. For insights into the catalyst surface properties, XPS spectra for Ni 2p, Ce 3d, and Si 2p of the reduced and passivated catalysts are shown in **Figure S6**. The Ni 2p spectra in **Figure S6**a indicates that, with an increase in SiO_2 concentration, the ratio of Ni^{2+} (attributed to NiO)[9,10] and Ni^0 (attributed to metallic Ni)[9,10] decreases. Thus, the presence of SiO_2 resulted in a greater presence of metallic Ni. The Ce 3d spectra in **Figure S6**b show that the ratio of Ce^{4+}/Ce^{3+} is similar across all samples: Ni/CeO_2: 3.71, $Ni/Ce_{0.9}Si_{0.1}O_2$: 4.10, $Ni/Ce_{0.8}Si_{0.2}O_2$: 3.81, $Ni/Ce_{0.2}Si_{0.8}O_2$: 4.23. The comparable oxidation state of Ce can be influenced by the oxygen passivation, after hydrogen reduction, in the catalyst pretreatment. The Si 2p spectra are provided in **Figure S6**c. Using the pretreated Ni/SiO_2 as reference, the peak at 104.1 eV can be attributed to Si in SiO_2. With the addition of CeO_2, a shift to lower binding energy is observed. It is also apparent that further increases in CeO_2 concentration result in corresponding increases in the binding energy. The increase can indicate interaction between the CeO_2 and SiO_2. A similar shift to higher binding energy was also observed in the XPS peaks for oxygen. The binding energy of both silicon and oxygen increase with the addition of CeO_2.

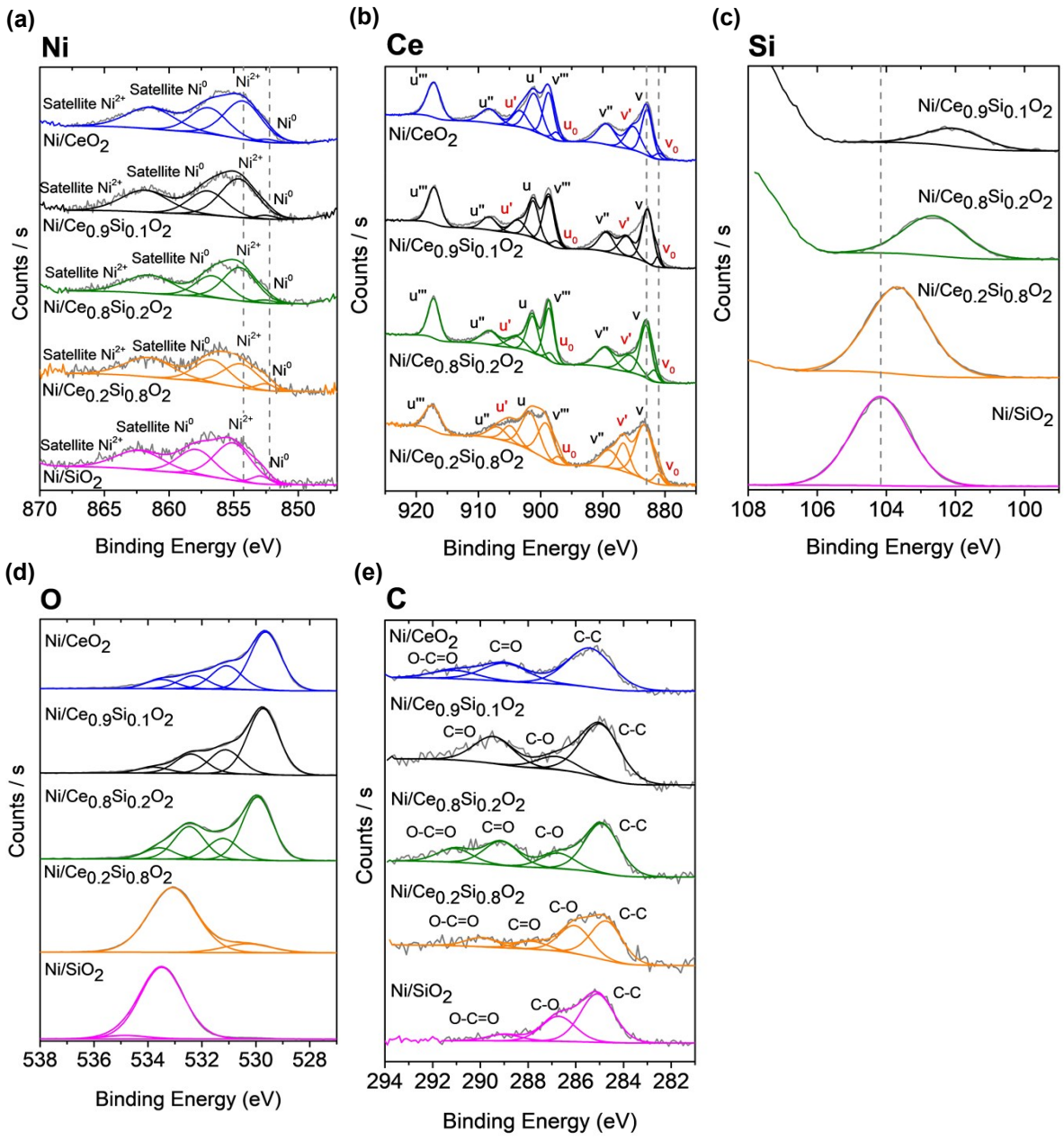

Figure S6 *XPS spectra of (a) Ni 2p; (b) Ce 3d; (c) Si 2p; (d) O 1s; and (e) C 1s for Ni/$Ce_xSi_yO_2$. With respect to the Ce 3d peaks, Ce^{3+} (red labels) are represented by u^0/v^0 and u'/v'; Ce^{4+} (black labels) are represented by u/v, u''/v'', and u'''/v'''.* [11,12] *The Ni/$Ce_xSi_yO_2$ were reduced and passivated prior to analysis. The deconvolutions of O 1s* [13,14] *and C 1s* [9,15,16] *were referenced to literature.*

The role of light in photothermal methanation

The carbon balance can be derived from the decoupled light and heat catalytic activity under continuous flow conditions. The balance was calculated as follows:

$$CO_2 + 4H_2 \rightleftharpoons CH_4 + 2H_2O$$

$$CO_2 + H_2 \rightleftharpoons CO + H_2O$$

The mol ratios of CO_2:CH_4 and CO_2:CO were 1:1 for both reactions. So as to demonstrate that carbon accumulation does not occur in the reaction, a sample case of the carbon balance is included. The flowrate of inlet CO_2 = 4 mL/min = 0.164 mmol/min and theoretically, the CH_4 outlet flowrate would be 0.164 mmol/min for 100% CO_2 conversion and CH_4 selectivity with no accumulation. Under thermal conditions, the CO_2 conversion of Ni/CeO_2 was 61.6% with CH_4 and CO selectivity of 97.3% and 2.7%, respectively at 400 °C. The molar flowrate of CO_2 at the outlet stream was calculated to 0.0631 mmol/min, based on CO_2 calibration. The product formation of CH_4 and CO were 0.0985 mmol/min and 0.0027 mmol/min, respectively. Therefore, the carbon balance was close to 100%. Additionally, carbon accumulation in the system was not observed and characterisation of selected spent catalyst indicated negligible change.

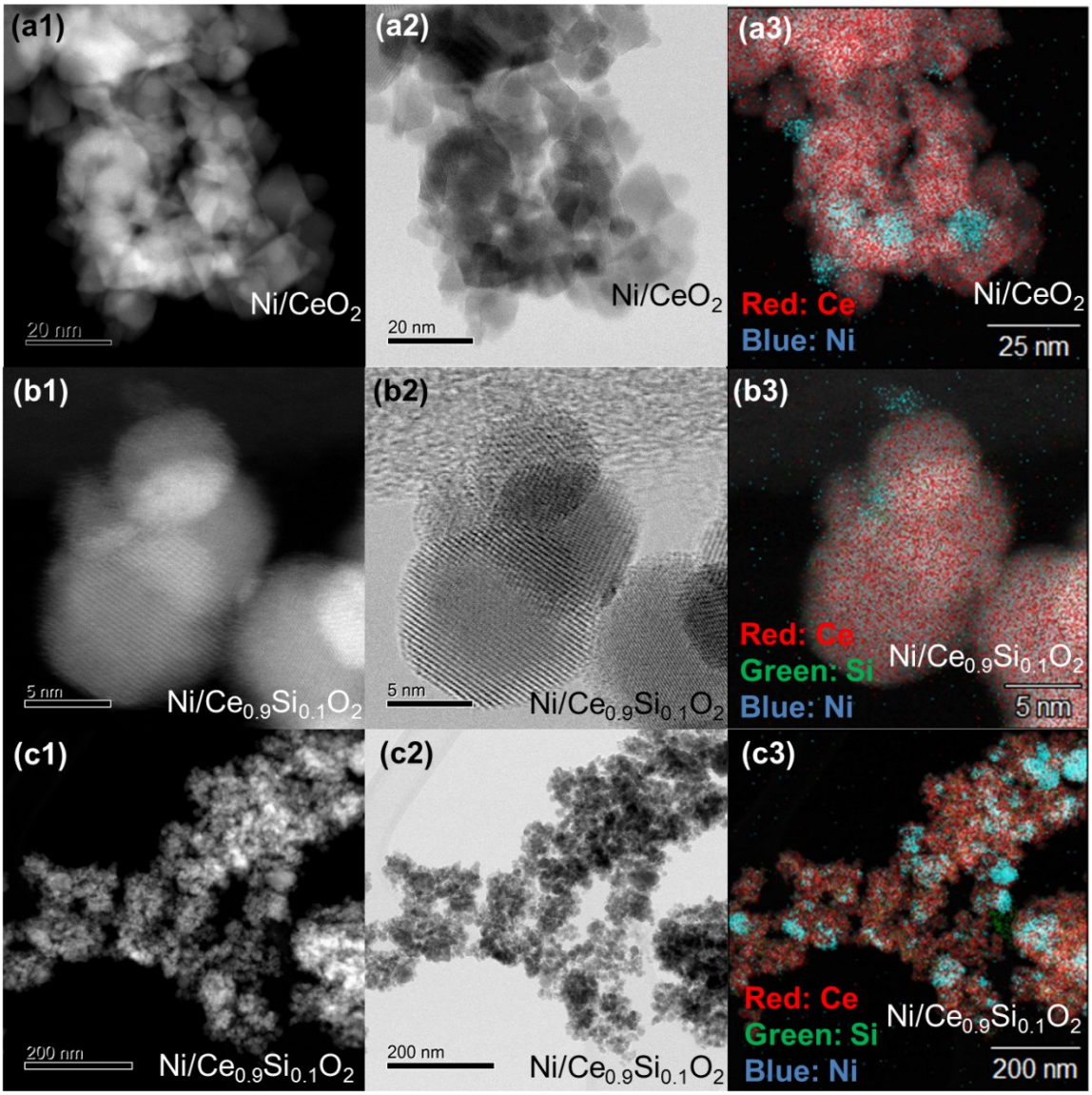

Figure S7 *TEM and EDS images of (a) Ni/CeO_2 and (b-c) $Ni/Ce_{0.9}Si_{0.1}O_2$. The figures include (1) dark field images, (2) bright field images, and (3) EDS mapping.*

Table S2 *Crystallite size of Ni and catalyst support for reduced and passivated and selected spent catalysts. The spent catalysts were collected after the decoupled activity tests under flow conditions.*

Catalyst	**Support (nm)**	**Ni (nm)**
Ni/CeO_2	12.2	13.8
Photo and Thermal: Ni/CeO_2	12.4	12.2
Ni/SiO_2	N/A	15.0
Thermal: Ni/SiO_2	N/A	15.8
Photo and Thermal: Ni/SiO_2	N/A	14.4

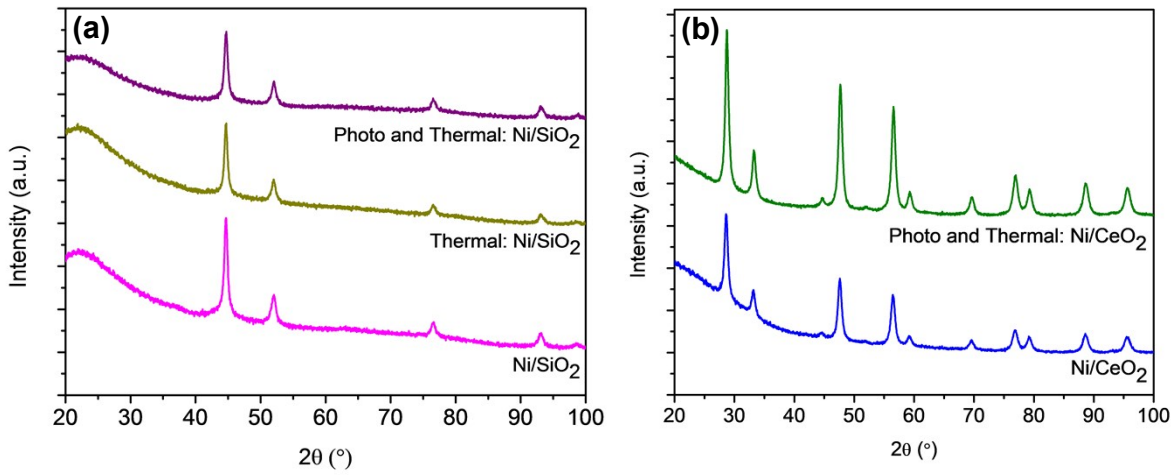

Figure S8 *XRD pattern of (a) Ni/SiO_2 and (b) Ni/CeO_2. The spent catalysts were collected after the decoupled activity tests (i) thermal and ii) photo and thermal) under flow conditions. The reduced and passivated catalysts (Ni/CeO_2 and Ni/SiO_2) are included for comparison.*

Exploring the different pathways over $Ni/Ce_xSi_yO_2$ via DRIFTS

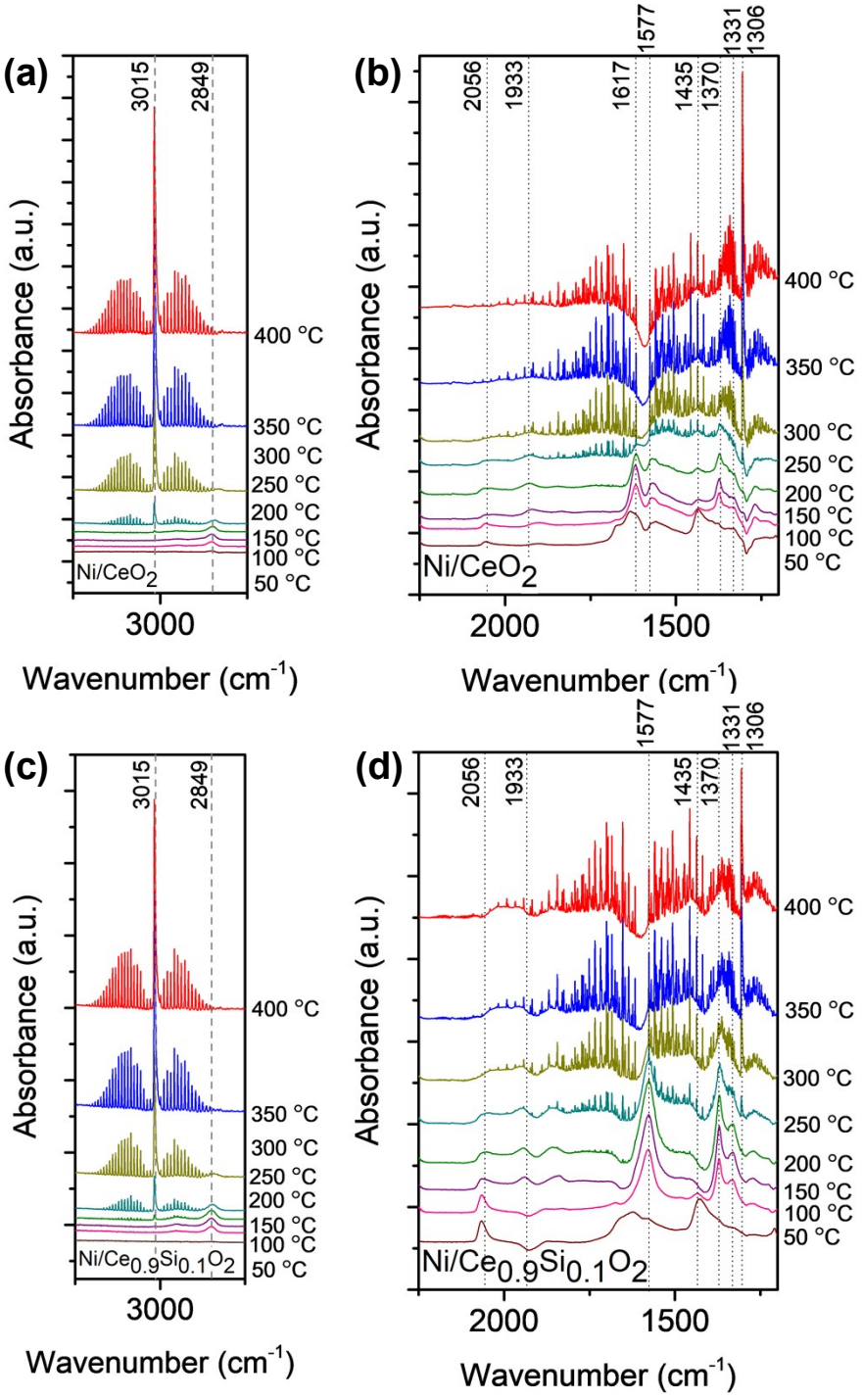

Figure S9 *DRIFTS spectra from 50 °C – 400 °C for Ni/CeO_2 and $Ni/Ce_{0.9}Si_{0.1}O_2$ from (a, c) 4000 – 2750 cm^{-1} and (b, d) 2250 – 1200 cm^{-1}.*

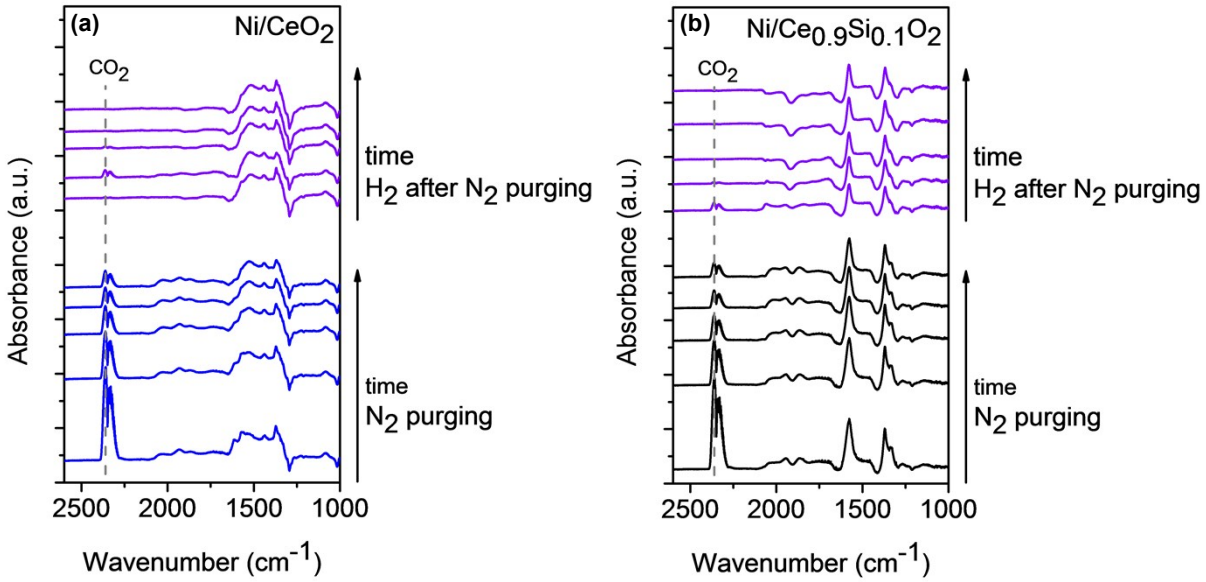

Figure S10 *DRIFTS transient spectra of (a) Ni/CeO_2 and (b) $Ni/Ce_{0.9}Si_{0.1}O_2$ at 200 °C under N_2 purging and H_2 flow after N_2 purge (purple lines) from 2600 – 1000 cm^{-1}. The spectra include the first five minutes of the gas transition stage. The CO_2 peak intensity and hydrogen carbonate peak (1617 cm^{-1}) of (a) Ni/CeO_2 decrease under N_2. In the case of (b) $Ni/Ce_{0.9}Si_{0.1}O_2$, intermediates were retained under the N_2 purge.*

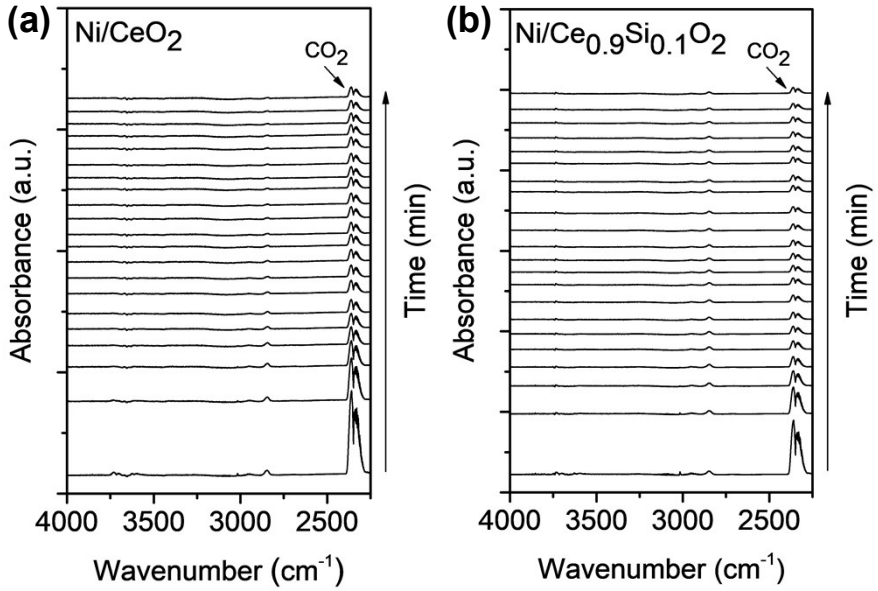

Figure S11 *DRIFTS transient spectra at 200 °C under N_2 purging at 4000 – 2250 cm^{-1} for (a) Ni/CeO_2 and (b) $Ni/Ce_{0.9}Si_{0.1}O_2$ collected under 1 min intervals. A decrease in CO_2 intensity of both samples were observed with time increase.*

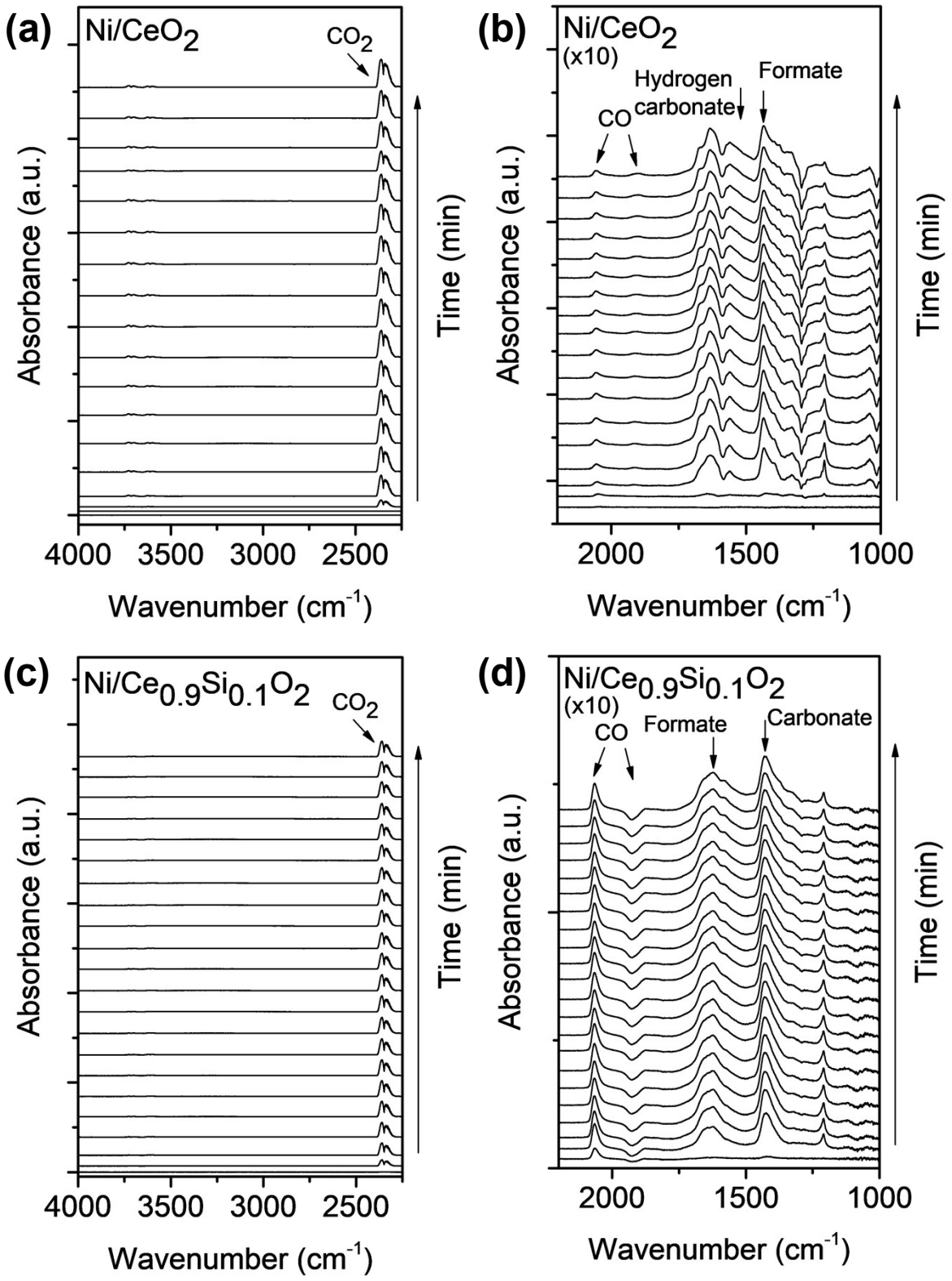

Figure S12 *Ni/CeO_2 and Ni/$Ce_{0.9}Si_{0.1}O_2$: DRIFTS transient spectra at 50 °C after introduction of CO_2 and H_2 at ratio of 1:4, diluted with N_2 (a,c) 4000 – 2250 cm^{-1} and (b,d) 2200 – 1000 cm^{-1}. The spectra was collected under 1 min intervals.*

References

1 S. Vivek, P. Arunkumar and K. S. Babu, *RSC Adv.*, 2016, **6**, 45947–45956.

2 B. M. Reddy, A. Khan, P. Lakshmanan, M. Aouine, S. Loridant and J. C. Volta, *J. Phys. Chem. B*, 2005, **109**, 3355–3363.

3 N. S. Arul, D. Mangalaraj and J. I. Han, *J. Mater. Sci. Mater. Electron.*, 2015, **26**, 1441–1448.

4 A. G. M. da Silva, H. V. Fajardo, R. Balzer, L. F. D. Probst, N. T. Prado, P. H. C. Camargo and P. A. Robles-Dutenhefner, *Chem. Eng. J.*, 2016, **286**, 369–376.

5 B. Liu, C. Li, G. Zhang, X. Yao, S. S. C. Chuang and Z. Li, *ACS Catal.*, 2018, **8**, 10446–10456.

6 A. N. Murashkevich, A. S. Lavitskaya, T. I. Barannikova and I. M. Zharskii, *J. Appl. Spectrosc.*, 2008, **75**, 730–734.

7 K. M. S. Khalil, L. A. Elkabee and B. Murphy, *J. Colloid Interface Sci.*, 2005, **287**, 534–541.

8 G. Bai, J. Wang, Z. Yang, H. Wang, Z. Wang and S. Yang, *RSC Adv.*, 2014, **4**, 47096–47105.

9 M. Gaboardi, A. Bliersbach, G. Bertoni, M. Aramini, G. Vlahopoulou, D. Pontiroli, P. Mauron, G. Magnani, G. Salviati, A. Züttel and M. Riccò, *J. Mater. Chem. A*, 2014, **2**, 1039–1046.

10 N. Wang, W. Qian, W. Chu and F. Wei, *Catal. Sci. Technol.*, 2016, **6**, 3594–3605.

11 G. Hua, L. Zhang, G. Fei and M. Fang, *J. Mater. Chem.*, 2012, **22**, 6851–6855.

12 L. Katta, P. Sudarsanam, B. Mallesham and B. M. Reddy, *Catal. Sci. Technol.*, 2012, **2**, 995–1004.

13 E. C. Lovell, J. Horlyck, J. Scott and R. Amal, *Appl. Catal. A Gen.*, 2017, **546**, 47–57.

14 X. Liao, Y. Zhang, M. Hill, X. Xia, Y. Zhao and Z. Jiang, *Appl. Catal. A, Gen.*, 2014, **488**, 256–264.

15 Y. Liu, Z. Wang, H. Zeng, C. Chen, J. Liu, L. Sun and W. Wang, *Mater. Lett.*, 2015, **142**, 280–282.

16 N. Díez, A. Śliwak, S. Gryglewicz, B. Grzyb and G. Gryglewicz, *RSC Adv.*, 2015, **5**, 81831–81837.